


# SCIENTIFIC REPORTS



OPEN

## Passively Q-switched Ytterbium-doped fiber laser based on broadband multilayer Platinum Ditelluride (PtTe<sub>2</sub>) saturable absorber

Ping Kwong Cheng<sup>1,2</sup>, Chun Yin Tang<sup>1,2</sup>, Xin Yu Wang<sup>1,2</sup>, Sainan Ma<sup>1,2</sup>, Hui Long<sup>1,2</sup> & Yuen Hong Tsang<sup>1,2</sup> 

Two-dimensional (2D) layered Platinum Ditelluride (PtTe<sub>2</sub>), a novel candidate of group 10 transition-metal dichalcogenides (TMDs), which provides enormous potential for pulsed laser applications due to its highly stable and strong nonlinear optical absorption (NOA) properties. PtTe<sub>2</sub> saturable absorber (SA) is successfully fabricated with firstly demonstrated the passively Q-switched laser operation within a Yb-doped fiber laser cavity at 1066 nm. Few layered PtTe<sub>2</sub> is produced by uncomplicated and cost-efficient ultrasonic liquid exfoliation and follow by incorporating into polyvinyl alcohol (PVA) polymer to form a PtTe<sub>2</sub>-PVA composite thin film saturable absorber. The highest achieved single pulse energy is 74.0 nJ corresponding to pulse duration, repetition rate and average output power of 5.2 μs, 33.5 kHz and 2.48 mW, respectively. This work has further exploited the immeasurable utilization potential of the air stable and broadband group 10 TMDs for ultrafast photonic applications.

Q-switching, a useful and very important technique, has been widely studied and applied in pulsed laser development over the past decades<sup>1–4</sup>. Contributed by the remarkable high pulse peak power, Q-switched laser can be employed in vast applications, for instance, industrial laser engraving, nonlinear optics, skin treatment, and eyes surgery<sup>5–7</sup>. Q-switched laser pulses can be produced by using Acousto-optical or Electro-optical modulators (AOM/EOM)<sup>8</sup> to actively modify the Quality factor within the cavity. However, AOM/EOM consists of bulky and expensive components, as well as the control driver. It will lead to high cost of production and complexity of the Q-switching laser system<sup>9</sup>. In contrast, modulates the cavity Q-factor passively by utilizing the nonlinear optical absorption (NOA) properties of some novel nano-materials may serve as an advanced alternative solution for Q-switched laser pulse generation.

Typically, doped crystals, e.g. Co: MALO<sup>10</sup> and V: YAG<sup>11</sup>, and semiconductor saturable absorber mirror (SESAM), e.g. InGaAs<sup>12</sup> are used to induce passively Q-switched laser operation among various commercial laser systems. However, the synthesis process of these commercial saturable absorbers usually involve expensive and complicated doped crystal growth and metal oxide chemical vapor deposition (MOCVD) techniques. Additionally, the narrow operation wavelength band of doped crystals and SESAMs also reduced the corresponding flexibility and applicability<sup>13</sup>. As a result, tremendous research effort has been devoted to searching novel saturable absorber materials which accompany with high operation performance and simple SA fabrication method. The carbon-based nano-materials e.g. graphene<sup>14</sup>, graphene-oxide<sup>15,16</sup>, and carbon nanotube<sup>17</sup> have attracted great research interests for its demonstrated exceptional nonlinear optical responses. However, these carbon-based materials have their own limitations e.g. lower modulation depth for graphene, diameter control needed for carbon nanotube. The study works on carbon-based materials have inspired the research interests of other layered 2D materials for pulsed laser and nonlinear optical applications.

<sup>1</sup>The Hong Kong Polytechnic University Shenzhen Research Institute, Shenzhen, Guangdong, China. <sup>2</sup>Department of Applied Physics and Materials Research Center, The Hong Kong Polytechnic University, Hung Hom, Kowloon, Hong Kong, China. Ping Kwong Cheng and Chun Yin Tang contributed equally. Correspondence and requests for materials should be addressed to Y.H.T. (email: [Yuen.Tsang@polyu.edu.hk](mailto:Yuen.Tsang@polyu.edu.hk))

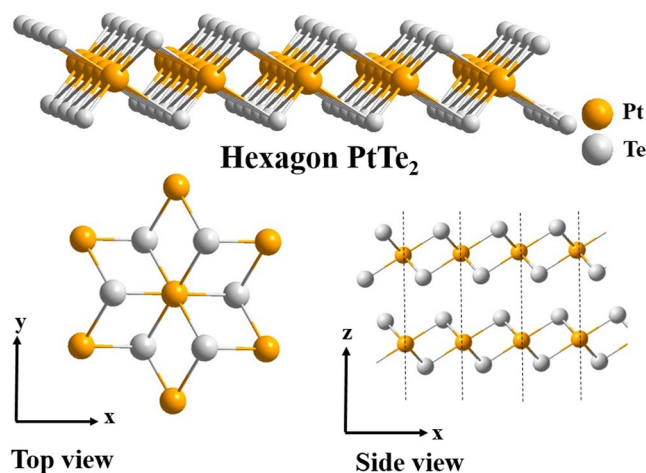


**Figure 1.** The 3D crystal structure of a monolayer PtTe<sub>2</sub>.

Transition metal dichalcogenide (TMD), a new class of the 2D family, had gained explosive growth of advertisement in the past few years. TMDs provided a wide choice of materials with various favorable properties<sup>18–20</sup> and which derived extensive applications, for example, photodetectors<sup>21</sup>, biosensors<sup>22</sup> and energy storage<sup>23</sup>. Layered TMD is composed of stacked planar crystal accompanied with a stoichiometry of MX<sub>2</sub>, where M and X stand for the group 4 to 10 transition metal and chalcogen atoms (S, Se, Te), respectively. Remarkably, the modification of NOA properties of TMDs nanosheet can be simply achieved by controlling the corresponding size, thickness<sup>24–26</sup> and concentration<sup>27</sup> which provided advance merit for utilizing in nonlinear optical (NLO) devices. In the recent years, the study of Q-switcher application is mainly focusing on the group 6 TMDs materials, such as MoS<sub>2</sub><sup>28</sup>, MoSe<sub>2</sub><sup>29</sup>, WS<sub>2</sub><sup>30</sup> and WSe<sub>2</sub><sup>31</sup>, but barely extend to the group 10 TMDs 2D materials. Reported by Zhou *et al.*<sup>32,33</sup>, PtS<sub>2</sub> had shown a strong interlayer interaction with a bandgap modulated from 0.25 eV to 1.6 eV, which even wider than that of black phosphorus (BP). Meanwhile, the air stability and electron carrier mobility (exceed 1000 cm<sup>2</sup>V<sup>-1</sup>s<sup>-1</sup>)<sup>32</sup> of group 10 TMDs also had shown superior result. The merits of the Pt-based 2D materials enable some new applications in different fields, e.g. photocatalyst<sup>34</sup>, FETs<sup>33</sup> and photodetectors<sup>35–38</sup>. Additionally, the Q-switched or mode-locked laser pulses generation have been successfully demonstrated by using PtS<sub>2</sub><sup>39,40</sup> and PtSe<sub>2</sub><sup>41–43</sup> based saturable absorber. For the infrared pulsed laser and optical communication application, the functional 2D material with a relatively small bandgap is more suitable for the mainstream laser photonic system<sup>41</sup>. Group 6 TMDs (e.g. monolayer WS<sub>2</sub>: 2.1 eV, 590 nm<sup>24</sup>; monolayer MoS<sub>2</sub>: 1.78 eV, 696 nm<sup>41</sup>) have relatively large bandgap and leads to the resonant absorption wavelength located in visible range. Although its bandgap energy can be further modified by changing the layer number, nanosheet size and lattice structure, however, it could further increase the optical loss and reduce stability of the system<sup>41</sup>. Previous studies had shown that monolayer and bilayer PtSe<sub>2</sub> are indirect bandgap of 1.18 eV and 0.21 eV<sup>44</sup>, respectively (semi-metallic as from 3 layers to bulk form). Remarkably, PtTe<sub>2</sub> shows the smallest monolayer indirect bandgap of 0.40 eV (~3 μm) among the Pt based TMDs family (it also exhibits semi-metallic as from bilayer to bulk form)<sup>44</sup>. These unique electronic structures of group 10 TMDs allow direct excitation of valence electrons to the conduction band, which it do not require the assistant of intermediate energy state (induced by lattice defect doping) in the band gap<sup>41</sup>. Hence it provided efficient and broadband saturable absorption within the infrared range covering the operational wavelengths of mainstream laser systems. Besides, compared with other 2D material based SAs with near or zero bandgap, such as WTe<sub>2</sub><sup>45</sup> or MXene (Ti<sub>3</sub>CN)<sup>46</sup>, PtTe<sub>2</sub> also shows advancing merits as mentioned previously. WTe<sub>2</sub> is very susceptible to oxidation in an ambient condition<sup>45,47</sup>, especially during the dispersion process. Usually, an additional protective coating or incorporated within host materials could curb the oxygen corrosion, but it requires additional surface treatment and passivation on the 2D material<sup>48</sup> which inevitably intervened the nonlinear optical properties of the SA. MXenes materials have the metal atoms that highly exposed on the surfaces<sup>49</sup>. In aqueous solutions of delaminated-MXene, literatures had shown that both the multilayered Ti<sub>3</sub>C<sub>2</sub>T<sub>x</sub> MXene and monolayer flakes<sup>50</sup> degrade gradually either in humid air<sup>51</sup> or water<sup>52</sup>. Meanwhile, to delaminate the MXene, a selective wet etching process is utilized to remove the “A” layer from the MXene MAX phase with followed by intercalation of the guest molecules (e.g. dimethyl sulfoxide -DMSO) and sonication, which highly hazardous Hydrofluoric acid (HF) is used as the wet etchant of the MXene MAX phase<sup>46</sup>. These complicated pre-SA preparation process and degradation problem will taper off the pragmatic application of MXene as a saturable absorber. Combined with the merits of high air stability and electron carrier mobility, group 10 TMDs are able to produce fast and stable nonlinear response to the incident light and generate narrower pulse width for the ultrafast operation<sup>43</sup>, therefore it provided a great potential for various nonlinear optics, pulsed laser and photonic applications.

In this work, we have firstly demonstrated the pulsed laser operation by using our homemade Platinum Ditelluride, PtTe<sub>2</sub> based saturable absorber. The 3D lattice structure of PtTe<sub>2</sub> is shown in Fig. 1. This newly developed Pt-based TMDs material has strong interlayer interaction<sup>53</sup> and air stability<sup>54,55</sup>. Contrast to the complicated and expensive CVD fabrication method<sup>53,56,57</sup>, the PtTe<sub>2</sub> nanosheets used for this experiment are produced by an uncomplicated and cost-effective ultrasonic liquid exfoliation technique and followed by incorporating within the

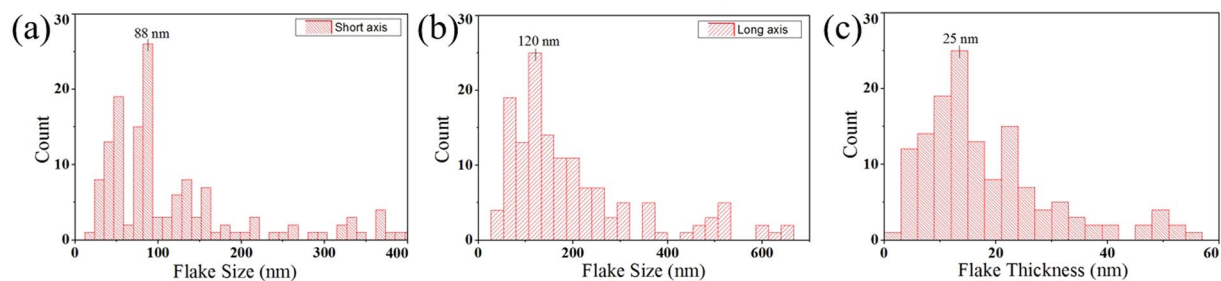


**Figure 2.** The statistical data of the AFM measurement among 150 PtTe<sub>2</sub> flakes with respect to the lateral dimensions of (a) short axis, (b) long axis, and (c) thickness of the PtTe<sub>2</sub> flakes.

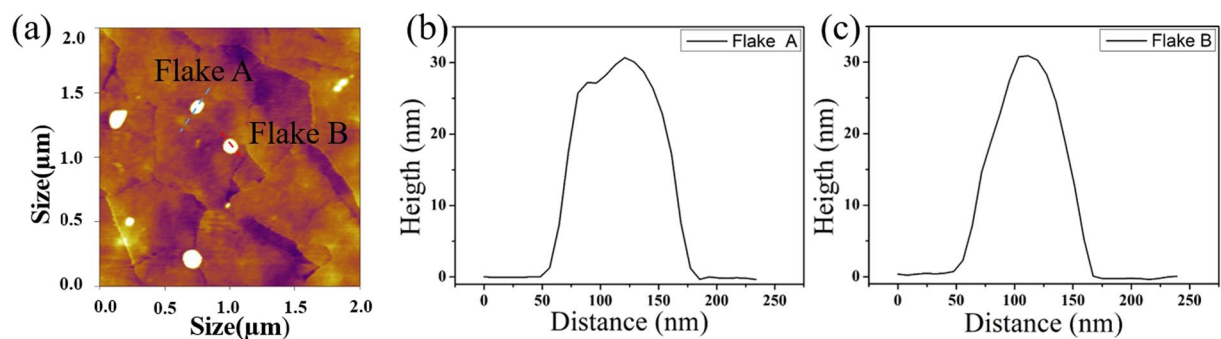


**Figure 3.** (a) AFM image of the fabricated PtTe<sub>2</sub> flakes. (b) The height profile recorded along the blue line of flake A and (c) the red line of flake B shown in (a).

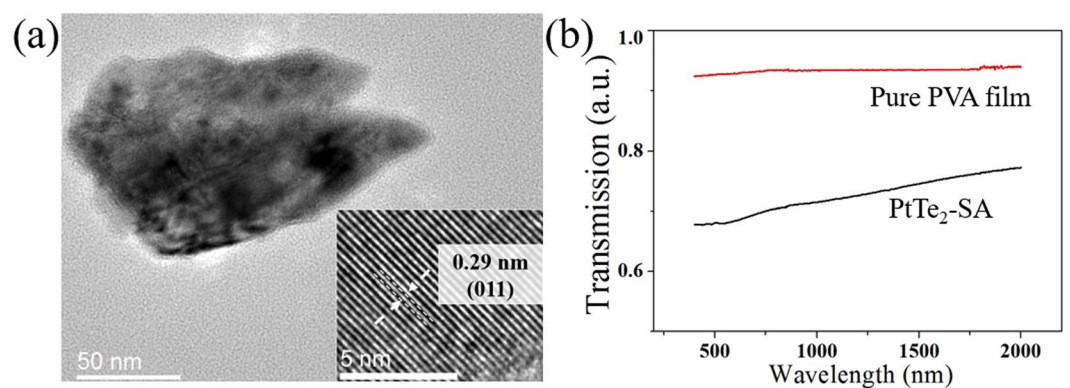


**Figure 4.** (a) The FETEM image of a PtTe<sub>2</sub> flake with inserted corresponding high-resolution FETEM image and (b) the Transmission spectrum of the PtTe<sub>2</sub>-SA.

polyvinyl alcohol (PVA) polymer to form a larger-scale PtTe<sub>2</sub>-PVA saturable absorber. The fabrication method employed here is well suitable for making commercial products.

## Result and Discussion

After successful ultrasonic liquid exfoliation, the morphology, crystal lattice structure and chemical composition of the obtained PtTe<sub>2</sub> nanosheets were characterized. Figure 2(a–c) show that the most frequently observed dimension along the short-axis, long-axis and thickness are around 88 nm, 120 nm, and 25 nm, respectively. Topology graph of two randomly selected flakes and their corresponding height profiles along the marked lines are shown in Fig. 3. The lateral dimensions for long-axis of both flake A and flake B are around 125 nm, which within the statistic result and indicated the successful exfoliation of the PtTe<sub>2</sub> sample.

From the TEM image (Fig. 4(a)), it shows that the lateral size of a randomly selected PtTe<sub>2</sub> flake well match with the AFM statistical results. The relevant high-resolution FETEM image is inserted in Fig. 4(a) and shows an inter-plane distance of 0.29 nm corresponding to the (011) plane of PtTe<sub>2</sub><sup>58</sup>. The Transmission spectra of the PtTe<sub>2</sub>-PVA composite and a reference PVA film are presented in Fig. 4(b) which shows that the type-II Dirac semimetal<sup>57</sup> PtTe<sub>2</sub> has no characteristic absorption peak from 500 nm to 2000 nm wavelength range, as similar

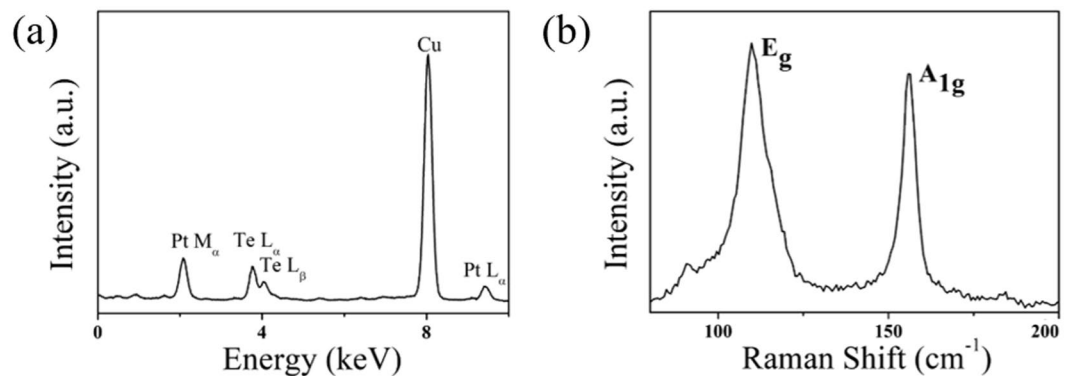


**Figure 5.** (a) The EDS spectrum and (b) Raman spectrum of the prepared PtTe<sub>2</sub> sample.

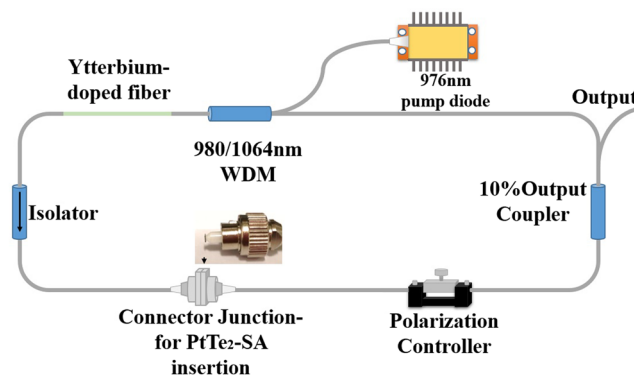


**Figure 6.** The schematic experimental setting of the passive Q-switching Yb-doped fiber laser.

to graphene-SA<sup>59</sup>. For the chemical composition of PtTe<sub>2</sub> sample, Fig. 5(a) shows only characteristic peaks from Pt or Te and no other observable impurities is found (Cu peak is induced from the copper mesh support for TEM measurement). Meanwhile, as shown in Fig. 5(b), the Raman-active modes E<sub>g</sub> and A<sub>1g</sub> were positioned at 110.7 cm<sup>-1</sup> and 154.8 cm<sup>-1</sup>, respectively, and which agree well with the previous report<sup>57</sup>. The E<sub>g</sub> mode is representing the in-plane vibration mode of Platinum and Ditelluride atoms. Meanwhile, the A<sub>1g</sub> is standing for the out-plane vibration modes of Ditelluride atoms. These strong characteristic Raman peaks reveal that the fabricated PtTe<sub>2</sub> nanosheets possess with good crystallinity.

For the laser test, a pure Polyvinyl alcohol (PVA) film, which possess of identical thickness as the PtTe<sub>2</sub>-PVA SA film, was first inserted between the connector junction of the ring cavity as shown in Fig. 6 to act as a control experiment set. No Q-switched laser pulses were observed by modifying the polarization direction of the polarization controller (PC) and pumping power. It confirms Q-switching operation cannot be obtained by using pure PVA polymer or cavity phase self-modulation. Further on, the fabricated PtTe<sub>2</sub>-SA was cut with a size in approximately 1 mm × 1 mm, and was introduced into the laser system by sandwiching between two fiber connectors. The parasitic reflection could be eliminated by using FC/APC connector and thus improved the stability of the Q-switching system.

Stable Q-switched pulse train was observed as the pump power elevated to the starting threshold of 118 mW. However, when the pump power raised beyond 146.5 mW, the Q-switched output was vanished due to the over saturation of the absorber at high input fluence<sup>26,60</sup>. The average output power was measured as from 1.03 mW to 2.48 mW with respect to the pump power from 118 mW to 146.5 mW as shown in Fig. 7(a). The modulation ranges of the pulse width (Full width at half maximum) and the repetition rate are 13.6 μs to 5.2 μs and 23.0 kHz to 33.5 kHz, respectively as shown in Fig. 7(b). The fluctuation of repetition rate and output power of the Q-switched laser are less than 5% within the test time of about 30 to 45 minutes during the measurement. The minimum pulse duration can be further shortened by either enhancing the modulation depth of the SA or reducing the total length of ring cavity<sup>61</sup>. The maximum recorded single pulse energy is about 74.0 nJ which is comparable to previous literature of passive Q-switching Yb-doped fiber laser with utilizing another TMDs based SA, for instance, MoSe<sub>2</sub> (116 nJ)<sup>29</sup>, MoS<sub>2</sub> (126 nJ)<sup>28</sup>, WS<sub>2</sub> (13.6 nJ)<sup>30</sup>, and even the group 10 PtS<sub>2</sub> (45.6 nJ) Q-switched laser operated in 1569 nm<sup>39</sup>. Meanwhile, the correlated pulse train, single laser pulse profile, radio-frequency (RF) (resolution bandwidth: 20 Hz) and wavelength spectra has shown in Fig. 7(c–f) corresponding to the maximum output single pulse energy of 74.0 nJ.

The passively Q-switched Yb-doped fiber laser based on PtTe<sub>2</sub> saturable absorber was first demonstrated. A stable Q-switched operation was illustrated from 1066 nm fiber ring cavity. The achieved pulse duration and repetition rate range are 13.6 μs to 5.2 μs and 23.0 kHz to 33.5 kHz, respectively, with correlated to the average output

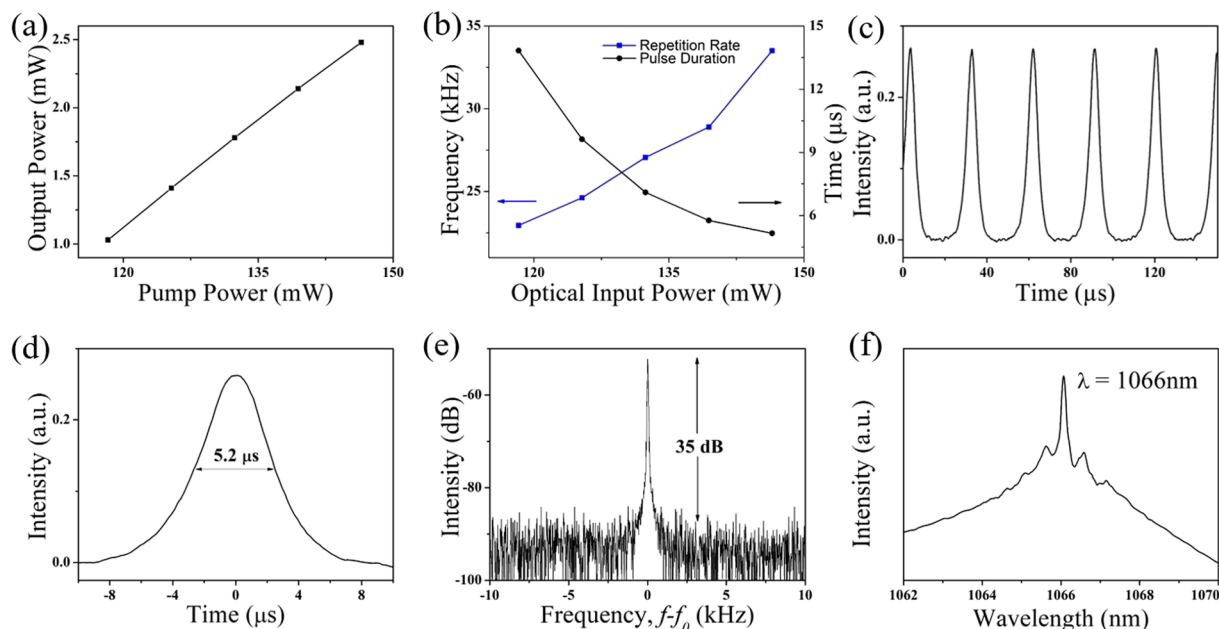


**Figure 7.** Q-switched laser performance: (a) The average output power and (b) Repetition rate and Pulse duration variation with respect to the different pump power. (c) Pulse train, (d) Single pulse profile, (e) Radio frequency spectrum, and (f) Wavelength spectrum corresponding to the maximum output single pulse energy of 74.0 nJ.

power from 1.03 mW to 2.48 mW. The highest achieved single pulse energy is 74.0 nJ which is well comparable with the output achieved by using other group 6 or 10 TMDs saturable absorber within the fiber laser system. This first demonstration proves the novel photonic applications of the newly developed 2D PtTe<sub>2</sub> material.

## Methods

**PtTe<sub>2</sub> nanosheets preparation.** The PtTe<sub>2</sub> nanosheets were prepared by using ultrasonic liquid exfoliation to break the interlayer bonding. Isopropyl Alcohol (IPA) was selected as the exfoliation solvent in order to prevent flakes aggregation because of its well surface energy compatibility with the TMDs substances. First, 175 mg PtTe<sub>2</sub> powder, which purchased from Six Carbon Inc., was mixed with 175 ml IPA solvent. Then, the mixture was probe sonicated for (SCIENTZ-1200E, Ningbo Scientz Biotechnology Co., Ltd) over 15 hours. The probe sonication operated at the frequency of 20 kHz and power of 1500 W. Then the PtTe<sub>2</sub> suspension was centrifuged at 3000 rpm speed for 5 minutes and only the supernatant was extracted to remove large flakes and impurities.

**Sample characterizations.** The statistic measurement of the size and thickness distribution among 150 flakes were obtained by utilizing an atomic force microscope (Bruker Nanoscope 8). The Ultrahigh magnification image and chemical ingredient of the PtTe<sub>2</sub> flakes were obtained by using field emission transmission electron microscopy (FETEM, JEM-2100F) with an accessory of energy-dispersive X-ray spectroscopy (EDS). Raman spectra was measured by a LabRAM HR 8000 Raman Spectrometer.

**PtTe<sub>2</sub> saturable absorber preparation.** In order to synthesize PtTe<sub>2</sub>-SA, firstly, PVA solution with 15% weight percentage was prepared by mixing the pure PVA powders with deionized water. Then the fabricated PtTe<sub>2</sub> suspension was added into the PVA solution by a weight ratio of 1: 6 and further stirred for 30 minutes. Afterward, the mixture was dried under 60 °C for 48 hours in the oven to form a PtTe<sub>2</sub>-PVA composite thin film and it serves as a transmission type saturable absorber for the Q-switching experiment.

**Experimental setup.** A ring cavity of Ytterbium-doped fiber laser was built as the schematic diagram shown in Fig. 6 for testing the performance of PtTe<sub>2</sub>-SA. The cavity was constituted with a 980/1064 wavelength division multiplexer (WDM), a 0.68 m long Yb-doped single mode fiber (LIEKKI Yb1200-4/125), a polarization-independent isolator (PI-ISO), a polarization controller (PC), and an output coupler with 90:10 coupling ratio. The total cavity length is about 12 meters. The fabricated PtTe<sub>2</sub>-SA was cut with a size in approximately 1 mm × 1 mm, and was introduced into the cavity by sandwiching between two fiber connectors.

## References

1. Degnan, J. J. Theory of the Optimally Coupled Q-Switched Laser. *IEEE J Quant Electron* **25**, 214–220, <https://doi.org/10.1109/3.16265> (1989).
2. Wagner, W. G. & Lengyel, B. A. Evolution of the Giant Pulse in a Laser. *J Appl Phys* **34**, 2040–2046, <https://doi.org/10.1063/1.1729732> (1963).

3. Szabo, A. & Stein, R. A. Theory of Laser Giant Pulsing by a Saturable Absorber. *J Appl Phys* **36**, 1562–1566, <https://doi.org/10.1063/1.1703087> (1965).
4. Xu, D., Wang, Y., Li, H., Yao, J. & Tsang, Y. H. 104 W high stability green laser generation by using diode laser pumped intracavity frequency-doubling Q-switched composite ceramic Nd: YAG laser. *Opt Express* **15**, 3991–3997, <https://doi.org/10.1364/OE.15.003991> (2007).
5. Watanabe, S. & Takahashi, H. Treatment of Nevus of Ota with the Q-switched Ruby Laser. *New England J. Medicine* **331**, 1745–1750, <https://doi.org/10.1056/NEJM199412293312604> (1994).
6. Qi, J., Wang, K. L. & Zhu, Y. M. A study on the laser marking process of stainless steel. *J Mater Proc Techno* **139**, 273–276, [https://doi.org/10.1016/S0924-0136\(03\)00234-6](https://doi.org/10.1016/S0924-0136(03)00234-6) (2003).
7. Latina, M. A., Sibayan, S. A., Shin, D. H., Noecker, R. J. & Marcellino, G. Q-switched 532-nm Nd: YAG laser trabeculoplasty (selective laser trabeculoplasty): A multicenter, pilot, clinical study. *Ophthalmology* **105**, 2082–2090, [https://doi.org/10.1016/S0161-6420\(98\)91129-0](https://doi.org/10.1016/S0161-6420(98)91129-0) (1998).
8. Tsang, Y. H., Qamar, F., King, T. A., Ko, D. K. & Lee, J. Nanosecond Q-switched operation of coupled Yb and Tm fibre lasers. *J Phys D: Appl Phys* **38**, 1365 (2005).
9. Leigh, M., Shi, W., Zong, J., Wang, J. & Jiang, S. Compact, single-frequency all-fiber Q-switched laser at 1  $\mu\text{m}$ . *Opt Lett* **32**, 897–899, <https://doi.org/10.1364/OL.32.000897> (2007).
10. Yumashev, K. V., Denisov, I. A., Posnov, N. N., Kuleshov, N. V. & Moncorge, R. Excited state absorption and passive Q-switch performance of  $\text{Co}^{2+}$  doped oxide crystals. *J Alloys and Comp* **341**, 366–370, [https://doi.org/10.1016/S0925-8388\(02\)00039-7](https://doi.org/10.1016/S0925-8388(02)00039-7) (2002).
11. Grabtchikov, S. *et al.* Passively Q-switched 1.35  $\mu\text{m}$  diode pumped Nd: KGW laser with V: YAG saturable absorber. *Opt Mater* **16**, 349–352, [https://doi.org/10.1016/S0925-3467\(00\)00099-9](https://doi.org/10.1016/S0925-3467(00)00099-9) (2001).
12. Spühler, G. J. *et al.* Experimentally confirmed design guidelines for passively Q-switched microchip lasers using semiconductor saturable absorbers. *J Opt Soc Am B* **16**, 376–388, <https://doi.org/10.1364/JOSAB.16.000376> (1999).
13. Tang, C. Y. *et al.* Passively Q-Switched Nd: YVO<sub>4</sub> Laser Using WS<sub>2</sub> Saturable Absorber Fabricated by Radio Frequency Magnetron Sputtering Deposition. *J Lightwave Techno* **35**, 4120–4124, <https://doi.org/10.1109/JLT.2017.2726138> (2017).
14. Luo, Z. *et al.* Graphene-based passively Q-switched dual-wavelength erbium-doped fiber laser. *Opt Lett* **35**, 3709–3711, <https://doi.org/10.1364/OL.35.003709> (2010).
15. Zhao, J. Q. *et al.* Graphene-oxide-based Q-switched fiber laser with stable five-wavelength operation. *Chin Phys Lett* **29**, 114206 (2012).
16. Zhao, J. *et al.* An Ytterbium-doped fiber laser with dark and Q-switched pulse generation using graphene-oxide as saturable absorber. *Opt Commun* **312**, 227–232, <https://doi.org/10.1016/j.optcom.2013.09.038> (2014).
17. Yu, H. *et al.* Sub-100 ns solid-state laser Q-switched with double wall carbon nanotubes. *Opt Commun* **306**, 128–130, <https://doi.org/10.1016/j.optcom.2013.05.010> (2013).
18. Mak, K. F. & Shan, J. Photonics and optoelectronics of 2D semiconductor transition metal dichalcogenides. *Nat Photon* **10**, 216, <https://doi.org/10.1038/nphoton.2015.282> (2016).
19. Chhowalla, M., Liu, Z. & Zhang, H. Two-dimensional transition metal dichalcogenide (TMD) nanosheets. *Chem Soc Rev* **44**, 2584–2586, <https://doi.org/10.1039/C5CS90037A> (2015).
20. Manzeli, S., Ovchinnikov, D., Pasquier, D., Yazyev, O. V. & Kis, A. 2D transition metal dichalcogenides. *Nat Rev Mater* **2**, 17033, <https://doi.org/10.1038/natrevmats.2017.33> (2017).
21. Zeng, L. H. *et al.* High-responsivity UV-vis photodetector based on transferable WS<sub>2</sub> film deposited by magnetron sputtering. *Sci Rep* **6**, 20343, <https://doi.org/10.1038/srep20343> (2016).
22. Gan, X., Zhao, H. & Quan, X. Two-dimensional MoS<sub>2</sub>: A promising building block for biosensors. *Biosens Bioelectron* **89**, 56–71, <https://doi.org/10.1016/j.bios.2016.03.042> (2017).
23. Jariwala, D., Sangwan, V. K., Lauhon, L. J., Marks, T. J. & Hersam, M. C. Emerging device applications for semiconducting two-dimensional transition metal dichalcogenides. *ACS nano* **8**, 1102–1120, <https://doi.org/10.1021/nn500064s> (2014).
24. Long, H. *et al.* Tuning nonlinear optical absorption properties of WS<sub>2</sub> nanosheets. *Nanoscale* **7**, 17771–17777, <https://doi.org/10.1039/C5NR04389A> (2015).
25. Liang, G. *et al.* Technique and model for modifying the saturable absorption (SA) properties of 2D nanofilms by considering interband exciton recombination. *J. Mater. Chem. C* **6**, 7501–7511, <https://doi.org/10.1039/C8TC00498F> (2018).
26. Chen, Y. *et al.* Mechanically exfoliated black phosphorus as a new saturable absorber for both Q-switching and Mode-locking laser operation. *Opt. Express* **23**, 12823–12833, <https://doi.org/10.1364/OE.23.012823> (2015).
27. Tao, L. *et al.* Fabrication of covalently functionalized graphene oxide incorporated solid-state hybrid silica gel glasses and their improved nonlinear optical response. *J. Phys. Chem. C* **117**, 23108–23116, <https://doi.org/10.1021/jp404463g> (2013).
28. Woodward, R. I. *et al.* Tunable Q-switched fiber laser based on saturable edge-state absorption in few-layer molybdenum disulfide (MoS<sub>2</sub>). *Opt. Express* **22**, 31113–31122, <https://doi.org/10.1364/OE.22.031113> (2014).
29. Woodward, R. I. *et al.* Wideband saturable absorption in few-layer molybdenum diselenide (MoSe<sub>2</sub>) for Q-switching Yb-, Er- and Tm-doped fiber lasers. *Opt. Express* **23**, 20051–20061, <https://doi.org/10.1364/OE.23.020051> (2015).
30. Zhang, M. *et al.* Yb- and Er-doped fiber laser Q-switched with an optically uniform, broadband WS<sub>2</sub> saturable absorber. *Sci Rep* **5**, 17482–17491, <https://doi.org/10.1038/srep17482> (2015).
31. Chen, B. *et al.* Q-switched fiber laser based on transition metal dichalcogenides MoS<sub>2</sub>, MoSe<sub>2</sub>, WS<sub>2</sub>, and WSe<sub>2</sub>. *Opt Express* **23**, 26723–26737, <https://doi.org/10.1364/OE.23.026723> (2015).
32. Zhao, Y. *et al.* Extraordinarily strong interlayer interaction in 2D layered PtS<sub>2</sub>. *Adv Mater* **28**, 2399–2407, <https://doi.org/10.1002/adma.201504572> (2016).
33. Zhao, Y. *et al.* High-Electron-Mobility and Air-Stable 2D Layered PtSe<sub>2</sub> FETs. *Adv Mater* **29**, 1604230, <https://doi.org/10.1002/adma.201604230> (2017).
34. Zhuang, H. L. & Henning, R. G. Computational Search for Single-Layer Transition-Metal Dichalcogenide Photocatalysts. *J. Phys. Chem. C* **117**, 20440–20445, <https://doi.org/10.1021/jp405808a> (2013).
35. Zeng, L. H. *et al.* Fast, Self-Driven, Air-Stable, and Broadband Photodetector Based on Vertically Aligned PtSe<sub>2</sub>/GaAs Heterojunction. *Adv. Funct. Mater.* **28**, 1705970, <https://doi.org/10.1002/adfm.201705970> (2018).
36. Zeng, L. H. *et al.* Ultrafast and sensitive photodetector based on a PtSe<sub>2</sub>/silicon nanowire array heterojunction with a multiband spectral response from 200 to 1550 nm. *NPG Asia Mater* **10**, 352–362, <https://doi.org/10.1038/s41427-018-0035-4> (2018).
37. Wu, D. *et al.* Design of 2D layered PtSe<sub>2</sub> heterojunction for the high-performance room-temperature broadband infrared photodetector. *ACS Photon* **5**, 3820–3827, <https://doi.org/10.1021/acsp Photonics.8b00853> (2018).
38. Zeng, L. H. *et al.* Controlled Synthesis of Two-dimensional Palladium Diselenide for Sensitive Photodetectors Application. *Adv Funct Mater* **29**, 1806878, <https://doi.org/10.1002/adfm.201806878> (2018).
39. Wang, X. *et al.* Laser Q-switching with PtS<sub>2</sub> microflakes saturable absorber. *Opt. Express* **26**, 13055–13060, <https://doi.org/10.1364/OE.26.013055> (2018).
40. Long, H. *et al.* Ultrafast laser pulses generation by using 2D layered PtS<sub>2</sub> as a saturable absorber. *J Lightwave Techno* **37**, 1174–1179, <https://doi.org/10.1109/JLT.2018.2889289> (2018).
41. Yuan, J. *et al.* Few-Layer Platinum Diselenide as a New Saturable Absorber for Ultrafast Fiber Lasers. *ACS Appl. Mater. Interfaces* **10**, 21534–21540, <https://doi.org/10.1021/acsmi.8b03045> (2018).

42. Tao, L. *et al.* Vertically standing PtSe<sub>2</sub> film: a saturable absorber for a passively mode-locked Nd: LuVO<sub>4</sub> Laser. *Photon Res* **6**, 750–755, <https://doi.org/10.1364/PRJ.6.000750> (2018).
43. Zhang, K. *et al.* Q-switched and mode-locked Er-doped fiber laser using PtSe<sub>2</sub> as a saturable absorber. *Photon Res* **6**, 893–900, <https://doi.org/10.1364/PRJ.6.000893> (2018).
44. Villaos, R. A. B. *et al.* Thickness dependent electronic properties of Pt dichalcogenides. *npj 2D Materials and Applications* **3**, <https://doi.org/10.1038/s41699-018-0085-z> (2019).
45. Koo, J. *et al.* Near-Infrared Saturable Absorption of Defective Bulk-Structured WTe<sub>2</sub> for Femtosecond Laser Mode-Locking. *Adv Funct Mater* **26**, 7454–7461, <https://doi.org/10.1002/adfm.201602664> (2016).
46. Jhon, Y. I. *et al.* Metallic MXene Saturable Absorber for Femtosecond Mode-Locked Lasers. *Adv Mater* **29**, 1702496, <https://doi.org/10.1002/adma.201702496> (2017).
47. Lee, C. H. *et al.* Tungsten Ditelluride: a layered semimetal. *Sci. Rep.* **5**, 10013, <https://doi.org/10.1038/srep10013> (2015).
48. Kopf, D. *et al.* All-in-one dispersion-compensating saturable absorber mirror for compact femtosecond laser sources. *Opt. Lett.* **21**, 486–488, <https://doi.org/10.1364/OL.21.000486> (1996).
49. Zhao, T., Zhang, S., Guo, Y. & Wang, Q. TiC<sub>2</sub>: a new two-dimensional sheet beyond MXenes. *Nanoscale* **8**, 233–242, <https://doi.org/10.1039/C5NR04472C> (2016).
50. Zhang, C. J. *et al.* Oxidation Stability of Colloidal Two-Dimensional Titanium Carbides (MXenes). *Chem. Mater.* **29**, 4848–4856, <https://doi.org/10.1021/acs.chemmater.7b00745> (2017).
51. Lipatov, A. *et al.* Effect of Synthesis on Quality, Electronic Properties and Environmental Stability of Individual Monolayer Ti<sub>3</sub>C<sub>2</sub> MXene Flakes. *Adv. Electron. Mater.* **2**, 1600255, <https://doi.org/10.1002/aelm.201600255> (2016).
52. Mashtalir, O. *et al.* Dye Adsorption and Decomposition on Two-Dimensional Titanium Carbide in Aqueous Media. *J. Mater. Chem. A* **2**, 14334–14338, <https://doi.org/10.1039/C4TA02638A> (2014).
53. Hao, S. *et al.* Low-Temperature Eutectic Synthesis of PtTe<sub>2</sub> with Weak Antilocalization and Controlled Layer Thinning. *Adv Funct Mater* **28**, 1803746, <https://doi.org/10.1002/adfm.201803746> (2018).
54. Ghosh, B. *et al.* Broadband excitation spectrum of bulk crystals and thin layers of PtTe<sub>2</sub>. *Phys. Rev. B* **99**, 045414, <https://doi.org/10.1103/PhysRevB.99.045414> (2019).
55. Politano, G. *et al.* Tailoring the Surface Chemical Reactivity of Transition-Metal Dichalcogenide PtTe<sub>2</sub> Crystals. *Adv Funct Mater* **28**, 1706504–1706511, <https://doi.org/10.1002/adfm.201706504> (2018).
56. Fu, L. *et al.* Highly Organized Epitaxy of Dirac Semi-metallic PtTe<sub>2</sub> Crystals with Extra High Conductivity and Visible Surface Plasmons at Edges. *ACS Nano* **12**, 9405–9411, <https://doi.org/10.1021/acsnano.8b04540> (2018).
57. Ma, H. *et al.* Thickness-Tunable Synthesis of Ultrathin Type-II Dirac Semimetal PtTe<sub>2</sub> Single Crystals and Their Thickness-Dependent Electronic Properties. *ACS Nanolett* **18**, 3523–3529, <https://doi.org/10.1021/acs.nanolett.8b00583> (2018).
58. Rosli, N. F. *et al.* Layered PtTe<sub>2</sub> Matches Electrocatalytic Performance of Pt/C for Oxygen Reduction Reaction with Significantly Lower Toxicity. *ACS Sustainable Chem. Eng.* **6**, 7432–7441, <https://doi.org/10.1021/acssuschemeng.7b04920> (2018).
59. Sun, Z. *et al.* Graphene Mode-Locked Ultrafast Laser. *ACS Nano* **4**, 803–810, <https://doi.org/10.1021/nn901703e> (2010).
60. Kiran, P. P. *et al.* Nonlinear absorption properties of 'axial-bonding' type tin (IV) tetratolylporphyrin based hybrid porphyrin arrays. *Opt Commun* **252**, 150–161, <https://doi.org/10.1016/j.optcom.2005.04.008> (2005).
61. Degnan, J. J. Optimization of passively Q-switched lasers. *IEEE J. Quantum Electron* **31**, 1890–1901, <https://doi.org/10.1109/3.469267> (1995).

## Acknowledgements

This work is financially supported by National Natural Science Foundation of China (61575167); Shenzhen Science and Technology Innovation Commission (JCYJ20170303160136888); Shenzhen Science and Technology Innovation Commission (JCYJ20180306173805740); The Research Grants Council of Hong Kong, China (GRF 152109/16E PolyU B-Q52T).

## Author Contributions

C.Y.T., P.K.C. and Y.H.T. developed the concept. C.Y.T. and P.K.C. conducted the experiments. P.K.C. and Y.H.T. wrote the paper. C.Y.T., P.K.C. and S.M. performed the laser characterization, A.F.M. and Raman measurement. X.Y.W. and H.L. conducted the TEM measurement. C.Y.T., P.K.C. and Y.H.T. reviewed and edited the manuscript. Y.H.T. directed the overall research. All authors read and approved the manuscript.

## Additional Information

**Competing Interests:** The authors declare no competing interests.

**Publisher's note:** Springer Nature remains neutral with regard to jurisdictional claims in published maps and institutional affiliations.



**Open Access** This article is licensed under a Creative Commons Attribution 4.0 International License, which permits use, sharing, adaptation, distribution and reproduction in any medium or format, as long as you give appropriate credit to the original author(s) and the source, provide a link to the Creative Commons license, and indicate if changes were made. The images or other third party material in this article are included in the article's Creative Commons license, unless indicated otherwise in a credit line to the material. If material is not included in the article's Creative Commons license and your intended use is not permitted by statutory regulation or exceeds the permitted use, you will need to obtain permission directly from the copyright holder. To view a copy of this license, visit <http://creativecommons.org/licenses/by/4.0/>.

© The Author(s) 2019